
Article:
Vallecchi, A., Langley, R. and Schuchinsky, A. (2016) Metasurfaces with Interleaved Conductors: Phenomenology and Applications to Frequency Selective and High Impedance Surfaces. IEEE Transactions on Antennas and Propagation, 64 (2). pp. 599-608. ISSN 0018-926X

https://doi.org/10.1109/TAP.2015.2511781

Metasurfaces with Interleaved Conductors: Phenomenology and Applications to Frequency Selective and High Impedance Surfaces

Andrea Vallecchi, Richard J. Langley, *Senior Member, IEEE,* and Alexander G. Schuchinsky, *Fellow, IEEE*

***Abstract*— A class of metasurfaces and high impedance surfaces (HIS) formed by doubly periodic arrays of interleaved conductors with sub-wavelength unit cells is proposed and discussed by way of example of the spiralled Brigid's cross arrangements. The main mechanisms underlying the distinctive features of these surfaces such as a broad fractional bandwidth (FBW), high angular and polarization stability and low loss are revealed and elucidated. It is demonstrated that all these salient characteristics of the interleaved arrays and HISs are attainable simultaneously being controlled by the pattern geometry. It is shown that the interleaved Brigid's cross HIS with truly sub-wavelength unit cells exhibits practically the same FBW and losses as square patch HIS with much larger unit cell. The effects of a dielectric substrate and near field confinement on the properties of intertwined Brigid's cross arrays are examined, and the analytical models provide insight into the performance of the discussed metasurfaces and HISs.**

***Index Terms*—Periodic structure, frequency selective surface, high impedance surface, metasurface, convoluted pattern, sub-wavelength resonance.**

I. Introduction

Periodic arrays utilised in conventional frequency selective surfaces (FSSs) [1] and high impedance surfaces (HISs) [2] are usually composed of the constituent elements confined to a single unit cell of size commensurate to half a wavelength at operational frequencies. As a result, their responses are narrowband and sensitive to a wave polarisation and incidence angle that hamper their application in low profile and conformal terminals. To alleviate these limitations, the use of convoluted and patterned conductors has been proposed in [3]-[5]. But the fractional bandwidth (FBW) of such FSSs became narrower.

To broaden the FBW of FSSs with small unit cells, it was proposed in [6] to extend the constitutive elements of periodic array beyond a single unit cell and interleave them into adjacent unit cells. While this approach enables broader FBW of the FSS with sub-wavelength unit cells, only very few geometries meet the stringent topological constraints on the compatible unit cell layout. To date just a handful of interwoven and tessellated conductor patterns have been reported in the literature for the FSSs [7]-[13] and HISs [6], [14] applications. Although feasibility of achieving fairly broad FBW at sub-wavelength unit cell size has been illustrated by simulations, the underlying physical mechanisms remain scarcely understood. This is especially concerned of the effects of unit cell topology and pattern tessellation on the array response which are essential for multiband and reconfigurable metasurfaces and HISs [12], [13].

In this paper, the properties of interleaved conductor arrays enabling the supreme performance of angular and polarisation stable FSSs and HISs are elucidated by way of the example of doubly periodic arrays of Brigid's crosses [15]. The paper is organised as follows. In Section II, the unique features of interleaved Brigid's cross metasurfaces are demonstrated and confirmed by the measurements. In Section III, the properties of compact HISs formed by the arrays of interwoven conductors are discussed, and it is shown for the first time that interleaved Brigid's cross HIS exhibits grossly superior angular and polarization stability than square patch HIS with practically the same FBW and losses. The main properties of stand-alone metasurfaces and HISs composed of periodic arrays of interleaved conductors are summarised in the Conclusion.

II. Interleaved Brigid's cross Arrays

The doubly periodic array of interleaved Brigid's crosses is illustrated in Fig. 1 by its fragment comprised of 3×3 unit cells. A primitive square unit cell of size p at the centre is outlined by dashed line. It contains a reference Brigid's cross (marked black) whose arms extend beyond the unit cell and interleave with the arms of all 8 Brigid's crosses (marked grey) centred in the surrounding unit cells. At each interweaving step N, four straight arm segments are added to the unit cell horizontally or vertically, as shown in Fig. 1 for $N = 1, 2, 3$ (at $N = 0$ all four arms are confined to a single unit cell only). At the steps $N \geq 4$, each extended arm is folded into a spiral spanning a quartet of adjacent unit cells. At every eighth step ($N = 7$, 15, and 23 in the layout of Fig. 1) each arm of the Brigid's cross re-enters a reference unit cell after completing a full turn of the spiral.

Manuscript received December 2014,…. This work was supported by the European Commission 7th Framework Program Marie Curie IAPP project grant no. 286333, "WiFEEB–Wireless Friendly Energy Efficient Buildings".

A. Vallecchi is with the Department of Engineering Science, University of Oxford, Oxford, OX1 3PJ, UK (e-mail: andrea.vallecchi@gmail.com). R. J. Langley is with the Department of Electronic and Electrical Engineering, University of Sheffield, Sheffield S1 3JD, UK (e-mail: r.j.langley@sheffield.ac.uk). A. G. Schuchinsky was with the School of Electrical and Electronic Engineering and Computer Science, Queen's University of Belfast, BT3 9DT, UK (e-mail: a.schuchinsky@ieee.org).

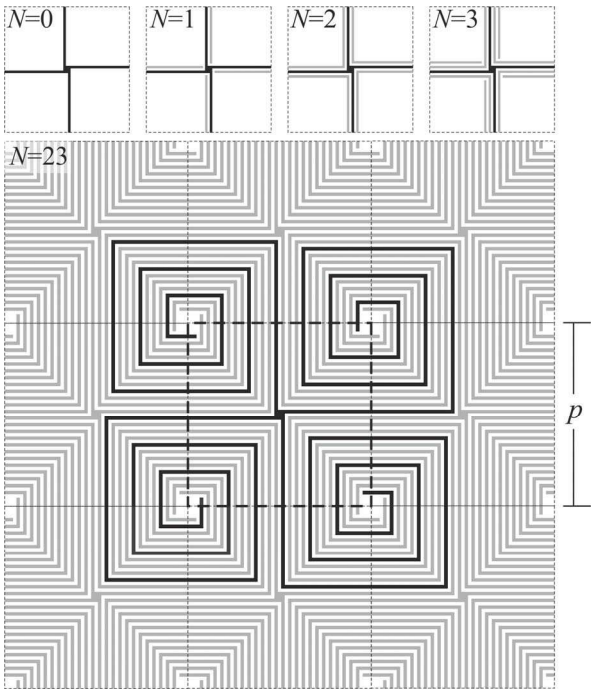

Fig. 1. Unit cell layout of the intertwined Brigid's cross array at variable number of the interleaved folds N=0, 1, 2, 3 (top), and N=23 (fully interleaved array). Marked black is the reference Brigid's cross and intertwined conductors arms extended from the adjacent unit cells are shown in grey.

Finally, arms of all eight Brigid's crosses surrounding the reference one are co-directionally wound in spirals.

The interleaved Brigid's cross arrays have been simulated in CST Microwave Studio (MWS) and cross-validated with Ansys HFSS and FEKO using the model of a single unit cell with periodic boundary conditions. The results obtained by the three entirely different full-wave (FW) methods, are in very good agreement, as illustrated in Fig. 2 for the fully interleaved array (N = 23 in Fig. 1) with unit cell size p = 10.8 mm, and strip conductor (s) and gap (g) widths s = g = 0.2 mm.

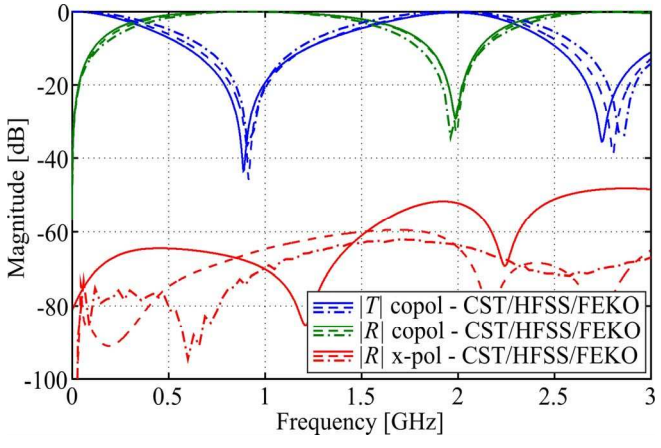

Fig. 2. The transmittance $|T|$ and reflectance $|R|$ of co-polar and cross-polar electric fields simulated for the array of fully interleaved Brigid's crosses in Fig. 1 (N=23) at normal incidence. The results from CST MWS (solid lines) are compared with HFSS (dashed lines) and FEKO (dash-dotted lines). The array periodicity is p = 10.8 mm, strip and gap widths are s=g=0.2 mm.

[1] FBW is defined as the rejection bandwidth at the transmittance level $|T|$ = –10 dB normalized to the resonance frequency f_r.

TABLE I
RESONANCE FREQUENCIES AND FBWS FOR FREE-STANDING INTERLEAVED ARRAYS WITH DIFFERENT CONDUCTOR PATTERNS. ALL ARRAY LAYOUTS HAVE PERIODICITY P = 10.8 MM, AND STRIP AND GAP WIDTHS S=G=0.2 MM

	Incidence	Interleaved Brigid's crosses		Interwoven convoluted crossed dipoles [7]	7-Fold entwined quadrifilar spirals [10]
		N=4	N=23		
f_r [GHz]	Normal	2.3	0.89	1.00	0.71
λ_r/p	Normal	12.1	31.2	27.8	39
Δf_r [%]	TE 45°	0.1	0	0.2	0.05
	TM45°	1.4	0.6	-0.2	-0.1
FBW_{10dB} [%]	Normal	75.4	71	63	55
	TE 45°	103	94	85	74.5
	TM 45°	52	48.6	46	40

A. Properties of the Fundamental Resonance

The characteristics of interleaved Brigit's cross arrays are summarised in Table I in comparison with the interwoven crossed dipoles [7] and entwined quadrifilar spirals [10] with unit cell of the same size. Inspection of Table I shows that frequency f_r of the fundamental resonance in the fully interleaved Brigit's cross array is lower than in interwoven crossed dipoles but higher than in entwined quadrifilar spirals. The high angular and polarisation stability of f_r proved to be an inherent property of all the arrays with interleaved conductor patterns and small unit cells with $p/\lambda_r \ll 1$ (λ_r is the wavelength at frequency f_r). The distinctive feature of Brigid's cross arrays is that at oblique incidence of TM waves the f_r deviation, Δf_r, becomes very small after the first few interleaving steps (N=4).

The FBW[1] of interleaved Brigid's cross arrays is not only broader than in the other interwoven array geometries but its dependence on the number N of interleaving folds qualitatively differs. Namely, in contrast to the intertwined quadrifilar spiral arrays where FBW grows monotonically with N [10], FBW of Brigid's cross arrays rapidly increases at the initial interleaving steps, reaching its peak at N = 4, and then slowly undulates near its maximum as illustrated in Fig. 3. This implies that the f_r of interleaved Brigid's cross arrays can be varied over broad frequency range with minor changes of FBW.

To elucidate the mechanisms underlying the broad FBW of

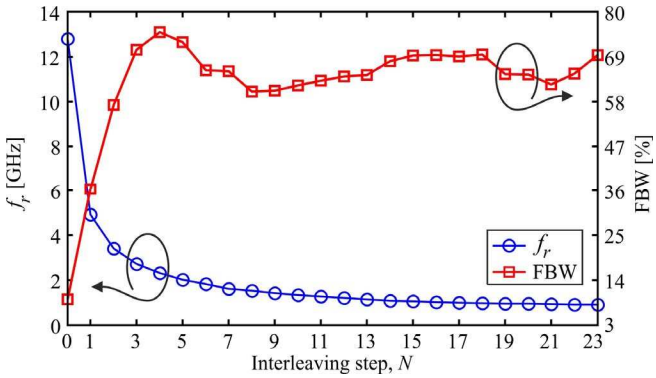

Fig. 3. Resonance frequencies and FBWs of the interleaved Brigid's cross arrays at variable number of arm folds. The array periodicity is p = 10.8 mm, and strip and gap widths are s=g=0.2 mm. Lines are for eye-guide only.

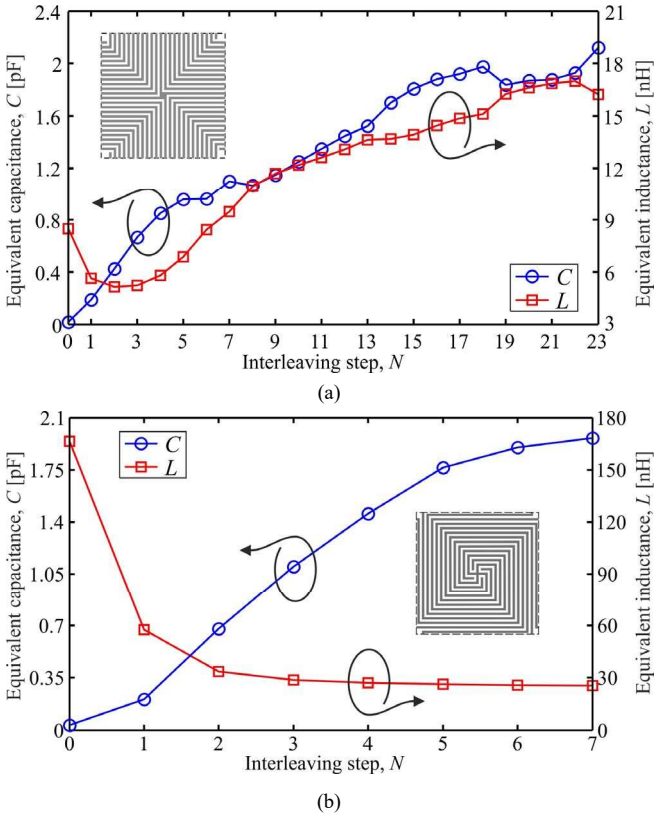

Fig. 4. Equivalent capacitance C and inductance L of the array unit cells with interleaved (a) Brigid's crosses and (b) quadrifilar spirals at different number of interwoven segments (N). Insets show unit cell layouts at full interleaving. The array periodicity is p = 10.8 mm, and strip and gap widths are s=g=0.2 mm. Lines are for eye-guide only.

the arrays with interleaved conductors, it is instructive to model a unit cell as a transmission line (TL) with a shunt reactance comprised of the series connected equivalent inductance L and capacitance C [1]. Then at the fundamental resonance

$$f_r = 1\Big/\left(2\pi\sqrt{LC}\right)$$
$$\mathrm{FBW} = \frac{\zeta_0}{6}\sqrt{\frac{C}{L}} \qquad (1)$$

where ζ_0 is the free-space impedance. The C and L, retrieved from the FW simulations of Brigid's crosses and intertwined spirals at variable number of interleaving steps N, are shown in Fig. 4 and demonstrate that the unit cell capacitances C of both layouts are commensurate and grow with N whereas the behaviour of inductances L qualitatively differs. Namely, in intertwined spirals, L is considerably higher but steadily decreases with N due to negative mutual inductance of the counter-directionally wound spiral arms. Alternatively, in Brigid's crosses only a few first arm folds are interleaved counter-directionally whereas at $N \geq 4$, the arms are folded into spirals co-directionally that increases L. Indeed, L of Brigid's crosses in Fig. 4 initially decreases with N, reaches its minimum and then grows along with C. Thus in accordance with (1), FBW reaches a maximum at the L minimum exhibits small undulations seen in Fig. 3 owing to different rates of C and L growth at $N > 4$ whilst f_r steadily decreases with N.

To provide a deeper insight in the properties of interleaved

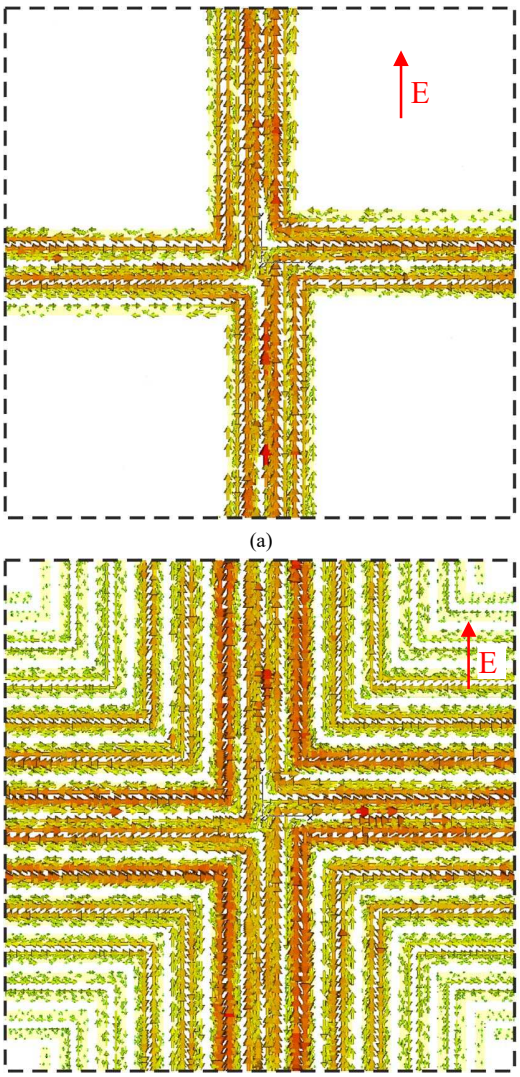

Fig. 5. Resonant current distributions in the unit cells of the Brigid's cross arrays with the parameters specified in Fig. 1 at different stages of interleaving: (a) N=4 and (b) N=23. The polarization of an incident field E_{inc} is vertical.

Brigid's cross arrays, the resonance currents in the unit cells at N=4 and N=23 interleaving steps (incident electric field is vertically polarized) are displayed in Fig. 5. These maps show that the horizontal arms carrying oppositely directed currents are responsible for the negative mutual inductance that initially decreases the overall unit cell inductance L. Currents on the arm folds with $N > 4$ have definitive directions, which are however opposite on adjacent strips. This results in a simultaneous increase of both L and C due to the prevailing self-inductance and strong capacitive coupling between the arms wound into spirals formed by the interleaved Brigid's crosses, cf. Fig. 1.

B. Effects of Dielectric Substrate

In practical arrangements of planar arrays, the patterned conductors are supported by substrates. The analysis of the free-standing interleaved Brigid's crosses above suggests that dielectric substrate may significantly affect the array response due to (i) increase of the unit cell equivalent capacitance and

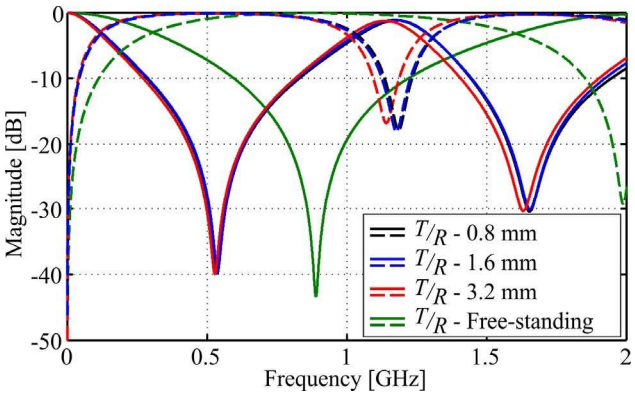

Fig. 6. Transmittance $|T|$ and reflectance $|R|$ at normal incidence on the fully interleaved (N=23) Brigid's cross array of Fig. 1 on dielectric substrate with permittivity ε_r = 4.9 and thicknesses: t_s = 0.8, 1.6, 3.2 mm. A square unit cell size: p = 10.8 mm, strips and gaps widths: s=g=0.2 mm, the conductor thickness: 17.5 μm.

(ii) reflectance at air-dielectric interface. To elucidate the substrate effect, the interleaved Brigid's cross arrays have been simulated at several values of substrate permittivity ε_r and thickness t_s. Fig. 6 demonstrates that in contrast to the conventional FSS [1], [16], even extremely thin substrates with $t_s \sim 2(s+g) \ll \lambda_s$, where λ_s is the wavelength in substrate at resonance frequency f_r, strongly influence the array response. Then at $t_s > 2(s+g)$, f_r and FBW of the fundamental resonance become practically invariant of t_s whilst $t_s < \lambda_s/2$. The latter feature proved to be an inherent property of the arrays with fine patterns of interleaved conductors, where the near-field is closely confined to the surface at the scale commensurate with the strip and gap widths. Fig. 7 illustrates such a localisation of the resonance electric field in the cross-section of a unit cell of fully interleaved Brigid's crosses on a dielectric substrate with thickness $t_s = 2\cdot(s+g) = 0.8$ mm and permittivity $\varepsilon_r = 4.9$.

The tight confinement and almost symmetric distribution of near-field about the array plane indicates its electrostatic nature. This implies that the effect of a dielectric substrate can be fairly accurately described by the effective permittivity

$$\varepsilon_r^{eff} = \frac{\varepsilon_r + 1}{2} \qquad (2)$$

Then the resonance frequency $f_r(\varepsilon_r)$ and FBW can be deduced using (1) where capacitance C is increased by factor ε_r^{eff} and inductance L remains unchanged by dielectric substrate:

$$f_r(\varepsilon_r) \approx \frac{f_r(\varepsilon_r = 1)}{\sqrt{\varepsilon_r^{eff}}}; \quad \mathrm{FBW}(\varepsilon_r) \approx \sqrt{\varepsilon_r^{eff}}\,\mathrm{FBW}(\varepsilon_r = 1) \qquad (3)$$

where $f_r(\varepsilon_r=1)$ and $\mathrm{FBW}(\varepsilon_r=1)$ are the resonance characteristics of the respective free-standing array.

The f_r and FBW of the interleaved Brigid's cross array on dielectric substrates calculated with (3) are summarised in Table II in comparison with the corresponding FW simulation data. Accuracy of approximations (3) is assessed by the percentage error (PCE): $PCE(x) = \left|1 - x(\varepsilon_r)/x(\mathrm{FW})\right| \times 100$, where x stands for either f_r or FBW. Inspection of Table II shows that $PCE(f_r)$ is less than 2% and only slightly increases with the substrate permittivity ε_r, whilst the approximate FBW gives a

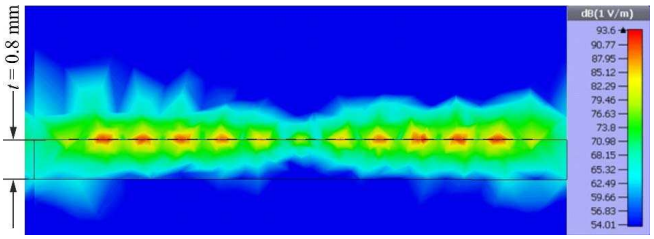

Fig. 7. Resonance electric field distribution in the cross section of two adjacent unit cells of the fully entwined (N=23) Brigid's cross array from Fig. 1 backed by a 0.8-mm-thick substrate with permittivity ε_r = 4.9. The array is illuminated by a normally incident plane wave.

proper qualitative trend but exhibits higher error. Discrepancy between the FW simulations and (3) can be partly attributed to overestimation of ε_r^{eff} by (2) which does not take into account the conductor thickness and the field crowding in the free-space gaps between the strip side walls. Additional error of FBW is caused by the reference values of L and C, deduced from the FW simulations at f_r and frequency f_b on the low-frequency slope of the resonance curve at $|T(f_b)|$ = -10 dB. As a result, the retrieved L and C values give fairly accurate estimates of f_r, whereas FBW is overestimated even for free-standing arrays and the error increases at higher permittivity ε_r, cf. Table II.

It is important to note that approximation (2) for ε_r^{eff} is valid normally for rather thick dielectric substrates with $t_s > \lambda_s/10$, but it becomes very sensitive to t_s of electrically thin substrates [16]. In contrast, the example of interleaved Brigid's cross arrays shows that (2) and (3) provide accurate estimates of f_r and FBW even for extremely thin substrates with $t_s < \lambda_s/200$.

C. *Experimental verification*

To verify the interleaved Brigid's cross array performance, test specimens were manufactured by photolithography and conductive inkjet printing and measured. The array comprised of 37×37 unit cells of size p = 7.5 mm each was fabricated on a square 277.5×277.5 mm^2 substrate of thickness 0.8 mm with a nominal dielectric constant $\varepsilon_r = 2.2 - j0.0009$ (Taconic TLY5). The unit cell contained interleaved Brigid's crosses with N=13 arm folds, strip and gap widths s=g=0.25 mm, and the conductor thickness 35 μm.

For the transmission measurements the specimen was fitted in a metallic frame placed between two Rohde and Schwarz HF906 wideband horns, connected to an HP8510C vector network analyser (VNA). The diffraction by the frame window was calibrated out first by the fixture measurement without

TABLE II
RESONANCE FREQUENCIES AND FBWS FOR THE INTERWOVEN BRIGIT'S CROSS ARRAY ON DIELECTRIC SUBSTRATES WITH PERMITTIVITIES ε_R = 1, 2.5, 3.38, 4.9. FW SIMULATIONS ARE COMPARED WITH APPROXIMATION (3) AT T_S = 0.8MM.

Substrate permittivity, ε_r		1	2.5	3.38	4.9
f_r	*FW*	0.9078	0.6972	0.624	0.5382
	Eq.(3)		0.6862	0.6134	0.5285
***PCE*(f_r) %**			1.573	1.693	1.795
FBW$_{10dB}$	*FW*	66.09	81.01	88.14	99.22
	Eq.(3)		87.43	97.81	113.5
***PCE* (FBW) %**			7.93	10.97	14.41

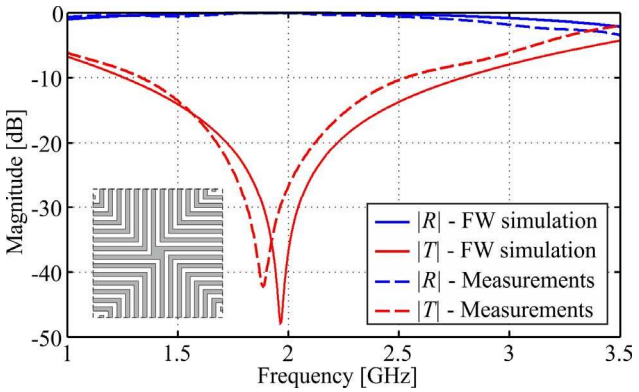

Fig. 8. Measured reflectance $|R|$ and transmittance $|T|$ of a finite array of interleaved Brigid's crosses vs. FW simulations of the corresponding infinite array. The unit cell, shown in the insert, comprises N=13 conductor folds and has size p = 7.5 mm; strip and gap widths are s=g=0.25 mm, and the conductor thickness is 35 μm. The array is printed on a 0.8-mm-thick dielectric substrate with permittivity $\varepsilon_r = 2.2 - j0.0009$ and has the size of 277.5x277.5 mm^2.

sample. Parasitic reflections including floor covered by absorbing material were undetectable in the measurements.

For reflectivity measurements, the same wide band horns were attached to a NRL (Naval Research Laboratory) arch [17], housed inside an anechoic chamber. The test specimen was mounted on a low density polystyrene table, surrounded by pyramidal absorbers. The setup was calibrated without sample and with a metal plate fitted instead of sample. The measurement accuracy was further enhanced by time gating used to separate the array response from the spurious back scattering caused by multipath propagation.

The measured transmission and reflection characteristics at normal incidence shown in Fig. 8 demonstrate good agreement with the FW simulations of the corresponding infinite array modelled in CST MWS using a single unit cell and the periodic boundary conditions.

III. Compact Broadband HIS

HISs, enabling the in-phase reflection, are the key elements of low-profile antennas with radiating elements placed closely to reflectors [2]. An ideal HIS acts as purely reactive surface with the reflection phase varying in the range [-90°, +90°] thus facilitating impedance matching and control of the antenna front-to-back radiation ratio, see, e.g. [18], [19]. Arrays of interwoven conductors with unit cells of substantially sub-wavelength size are particularly instrumental for compact HISs with high angular and polarisation stability and broad FBW [6], [14]. Also, their near-field confinement to a close proximity of the surface can significantly reduce parasitic couplings between HIS constituent elements and radiators of low profile antennas.

The unique features of interleaved Brigid's cross arrays discussed in Section II make them especially appealing for compact HISs. In particular, the possibility of varying f_r over a broad frequency range with a minor change of FBW, cf. Fig. 3, is essential for reconfigurable HIS where the operating frequency could be adjusted almost independently from FBW[2] by altering the length of interleaved arms.

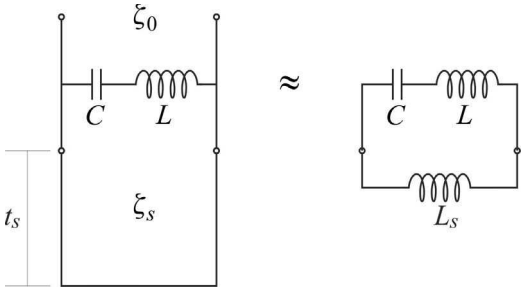

Fig. 9. TL model of a HIS unit cell composed of interwoven Brigid's cross arrays backed by a substrate with characteristic impedance ζ_s, and its corresponding equivalent lumped circuit on the right.

A. HIS analysis

HIS, composed of an interleaved conductor array on thin grounded substrate, has substantially sub-wavelength unit cell, and is fairly accurately described by the TL model [20] shown in Fig. 9. The FBW, defined by the frequencies at which the HIS impedance equals $\pm j\zeta_0$, can be represented in the form[3]

$$\mathrm{FBW_{HIS}} = \frac{2}{\omega_{r\mathrm{HIS}}}\left[\sqrt{-Q}\cos\left(\frac{\varphi}{3}\right)+\frac{A_2}{3}\right] \tag{4}$$

where $\omega_{r\mathrm{HIS}} = 2\pi f_{r\mathrm{HIS}} = 1/\sqrt{C(L+L_s)}$ is a centre frequency corresponding to the zero reflection phase; C and L are the equivalent capacitance and inductance of a unit cell in stand-alone array in the medium with the effective permittivity ε_r^{eff}; $L_s \approx \mu_0 t_s$ is inductance of a TL section of length $t_s \ll \lambda_s$ and μ_0 is the free-space permeability;

$$Q = \frac{3A_1 - A_2^2}{9};\quad \varphi = \arccos\left(\frac{R}{\sqrt{-Q^3}}\right);\qquad R = \frac{9A_1A_2 - 27A_0 - 2A_2^3}{54} \tag{5}$$

$$A_2 = -\zeta_0\frac{L+L_s}{L_sL};\quad A_1 = -\frac{1}{LC};\quad A_0 = \frac{\zeta_0}{L_sLC} \tag{6}$$

The $f_{r\mathrm{HIS}}$ and $\mathrm{FBW_{HIS}}$, computed with the aid of (4), are shown in Fig. 10 in comparison with the FW simulations of the HIS composed of the interleaved Brigid's crosses on grounded substrates with permittivity ε_r =2.2 and thicknesses $t_s = \lambda_{r\mathrm{HIS}}/20$, where $\lambda_{r\mathrm{HIS}}$ is a free-space wavelength at frequency $f_{r\mathrm{HIS}}$[4]. An excellent agreement between the TL model and FW simulations obtained for both $f_{r\mathrm{HIS}}$ and $\mathrm{FBW_{HIS}}$ at variable number of arm folds proves that the equivalent lumped capacitance C and inductance L adequately represent the unit cell reactance. It is also noteworthy that $f_{r\mathrm{HIS}}$ and $\mathrm{FBW_{HIS}}$ in Fig. 10 follow the same trends as f_r and FBW of the free-standing

[2] The HIS bandwidth is defined as the frequency band where impedance magnitude is higher than the free-space impedance ζ_0 that corresponds to the phase variation of the HIS reflection coefficient in the range [-90°, +90°] [2].

[3] Eqn. (4) for FBW is obtained from the standard solution of cubic equation [21]. Similar eqn. (5) for FBW in [19] proved to be incorrect whilst plots in Fig. 3 of [20] fully correlate with the FBW calculated by eqn. (4) of this paper.

[4] For consistent comparison of the HIS performance at different centre frequencies $f_{r\mathrm{HIS}}$, the electrical thickness of substrates was fixed at $t_s = \lambda_{r\mathrm{HIS}}/20$.

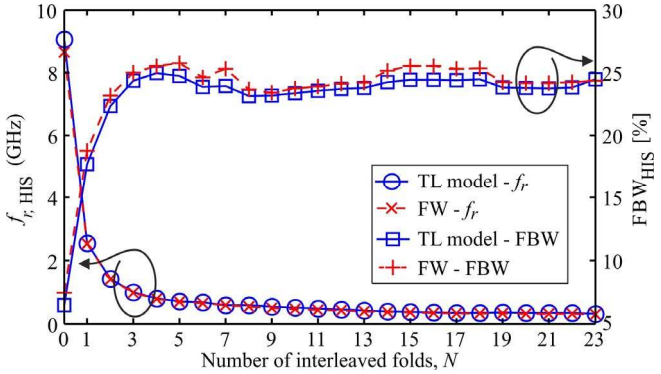

Fig. 10. Resonance frequencies $f_{r\mathrm{HIS}}$ and FBW$_{\mathrm{HIS}}$ computed by the TL model (circles) and FW simulations in CST MWS (crosses) for the HIS composed of interleaved Brigid's cross arrays with different number of arm folds supported by a grounded substrate with permittivity $\varepsilon_r = 2.2$ and thickness $t_s = \lambda_{r\mathrm{HIS}}/20$. The array periodicity is $p = 10.8$ mm; strip and gap widths are s=g=0.2 mm. Lines are for eye-guide only.

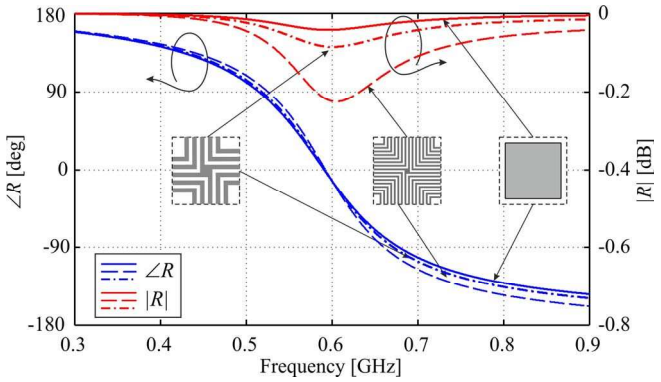

Fig. 11. Reflectance at normal incidence onto HISs composed of interleaved Brigid's crosses with N=15 and N=4 arm folds vs. square patches. All the HISs have the resonance frequencies $f_{r\mathrm{HIS}} \approx 0.59$ GHz at the same gaps $g = 0.15$ mm, and substrate thickness $t_s = 22.4$ mm and permittivity $\varepsilon_r = 2.2 - j0.0009$.

Brigid's cross arrays in Fig. 3 even for the HIS with very thin substrates. This provides further evidence of the tight near-field confinement to the patterned conductor as in the stand-alone array, cf. Fig. 7.

B. Performance of interleaved Brigid's cross HISs

HISs formed by arrays of interleaved conductors and square patches normally operate at very disparate frequencies due to incommensurate size of their unit cells and ratios $\lambda_{r\mathrm{HIS}}/p$. Nonetheless it is instructive to compare their performance at the same centre frequency. The HISs composed of square patches and interleaved Brigid's crosses on grounded dielectric substrates with permittivity $\varepsilon_r = 2.2 - j0.0009$ and thickness $t_s = 22.4$ mm have been designed for a centre frequency $f_{r\mathrm{HIS}} \approx 0.59$ GHz ($\lambda_{r\mathrm{HIS}}/t_s \sim 23$). A reference square patch unit cell has the size $p = 48$ mm ($\lambda_{r\mathrm{HIS}}/p \approx 10.6$) and a gap between adjacent patches $g = 0.15$ mm. The two configurations of fully interleaved Brigid's crosses had the same gap $g = 0.15$ mm between adjacent strips whilst the unit cell size p and strip width s were adjusted to keep $f_{r\mathrm{HIS}}$ unchanged. In one layout, the unit cell size is $p = 7.8$ mm ($\lambda_{r\mathrm{HIS}}/p \approx 65$), and it contains N=15 arm folds with strip width $s = 0.22$ mm. The other unit cell layout contains only $N = 4$ arm folds with wider strips, $s = 2.7$ mm, and has larger size $p = 18$ mm ($\lambda_{r\mathrm{HIS}}/p \approx 28$) which is still more than 2.5 times smaller than the reference square patch unit cell. All conductors are copper foil of thickness 17.5 μm.

The reflection coefficients, simulated in CST MWS for the centre frequency $f_{r\mathrm{HIS}} \approx 0.59$ GHz, are shown in Fig. 11. They demonstrate that fully interleaved Brigid's cross HISs with the smaller ($p = 7.8$ mm) and larger ($p = 18$ mm) unit cells have FBW$_{\mathrm{HIS}} \approx 23\%$ and 26%, respectively, that are only marginally narrower than the 27.7% for the square patch HIS with $p = 48$ mm. For comparison, the HIS formed by interdigitated fingers in the unit cell of similar size, $p = 13.5$ mm, still has a narrower FBW of 21.3% [14].

Slightly higher resonance losses in the fully interleaved Brigid's cross HIS than in patch HIS are attributed to the close confinement of near-field to the fine pattern of interleaved conductors. These losses markedly decrease at a lesser number of arm folds N at the expense of larger unit cell or higher $f_{r\mathrm{HIS}}$.

Taking into account that $f_{r\mathrm{HIS}}$, FBW and losses of interleaved Brigid's cross HIS can be altered somewhat independently, a judicious trade-off between the unit cell size and the number of arm folds allows FBW and losses to be nearly the same as in patch based HIS as illustrated by the example in Fig. 11. At the same time, substantially smaller unit cells of the HIS with interleaved conductors enable their superior angular and polarisation stability as elucidated next.

C. Polarisation and Angular Stable HIS

The angular and polarisation stability proved to be an inherent property of a fundamental resonance in the stand-alone arrays of interleaved conductors with sub-wavelength unit cells, cf. [6]-[12], [22] and Table 1 above. However, the HIS formed by such arrays on grounded dielectric substrates are polarisation sensitive, viz. $f_{r\mathrm{HIS}}$ remains stable in a broad range of incidence angles θ only for TE polarised waves but varies significantly for TM waves. Fig. 12 illustrates this effect for HIS composed of interleaved Brigid's crosses, and similar behaviour has been observed in the HIS with other unit cell geometries, cf. [6], [14]. This disparity in the HIS responses to TE and TM waves is solely caused by the additional phase accrued by the TM wave in the thin substrate between the conductor array and ground.

Angular stability of $f_{r\mathrm{HIS}}$ for incident TM waves can be restored using a substrate studded with thin pins connecting the array conductors to ground [3], [23]-[24]. A fragment of such a modified HIS composed of interleaved Brigid's crosses is shown in inset to Fig. 13 which illustrates an excellent angular stability of $f_{r\mathrm{HIS}}$ for incident TM waves. To elucidate the mechanism of the TM wave reflectance from the modified HIS, it is instructive to treat the pin studded substrate as a slab of wire-medium. The latter approach, detailed in Appendix, is particularly apt for the HIS formed by the interwoven conductor arrays with substantially subwavelength size of the unit cells. Indeed, the incident TM wave cannot propagate in such a dense wire-medium slab but it excites TEM waves travelling along the wires. The phase accrued by the TEM waves in the slab does not depend on the angle of incidence of the TM wave, so the phase of the TM wave reflected from the grounded layer of wire-medium does not change with θ either.

Pins embedded into HIS substrate have negligible effect on

the TE wave reflectance because the electric field of the TE wave is perpendicular to the wires and does not interact with them. Also, the input impedance of the TE wave incident on a thin grounded dielectric slab is practically invariant of θ in a broad range of incidence angles [23]. Therefore the response of the modified HIS to incident TE waves remains the same as in the case of the HIS without pins in the substrate as shown in Figs. 12 (c)-(d).

The HIS, composed of the interleaved conductor arrays on thin dielectric substrate with thin pins embedded in the centre of each unit cell, can be modelled with an aid of the equivalent circuit in Fig. 9 where the reactance of a unit cell in interleaved conductor array is connected in parallel with the reactance of a grounded wire-medium slab. Thus, owing to the substantially sub-wavelength size of the array unit cell, its intrinsic reactance remains nearly constant in a broad range of θ as shown for the stand-alone interleaved Brigid's crosses in Section II and for intertwined spirals in [22]. Since both constituent reactances of the unit cell are practically invariant of θ, f_{rHIS} of such HIS exhibits high angular and polarisation stability.

In contrast to f_{rHIS}, FBW_{HIS} and attenuation vary noticeably with incidence angle θ as evident in Figs. 12, 13. Moreover, at the same polarisation of incident wave, the dependences of $FBW_{HIS}(\theta)$ are inverse to $FBW(\theta)$ for the same stand-alone conductor arrays, i.e. FBW_{HIS} is broader for the TM waves than for the TE waves and it broadens with θ, whereas FBW_{HIS} narrows for the TE waves. Such a behaviour of the FBW_{HIS} originates in duality of the TE and TM wave reflectance and transmittance by thin conductor screens. This implies that the FBW_{HIS} is primarily determined by the array transmittance

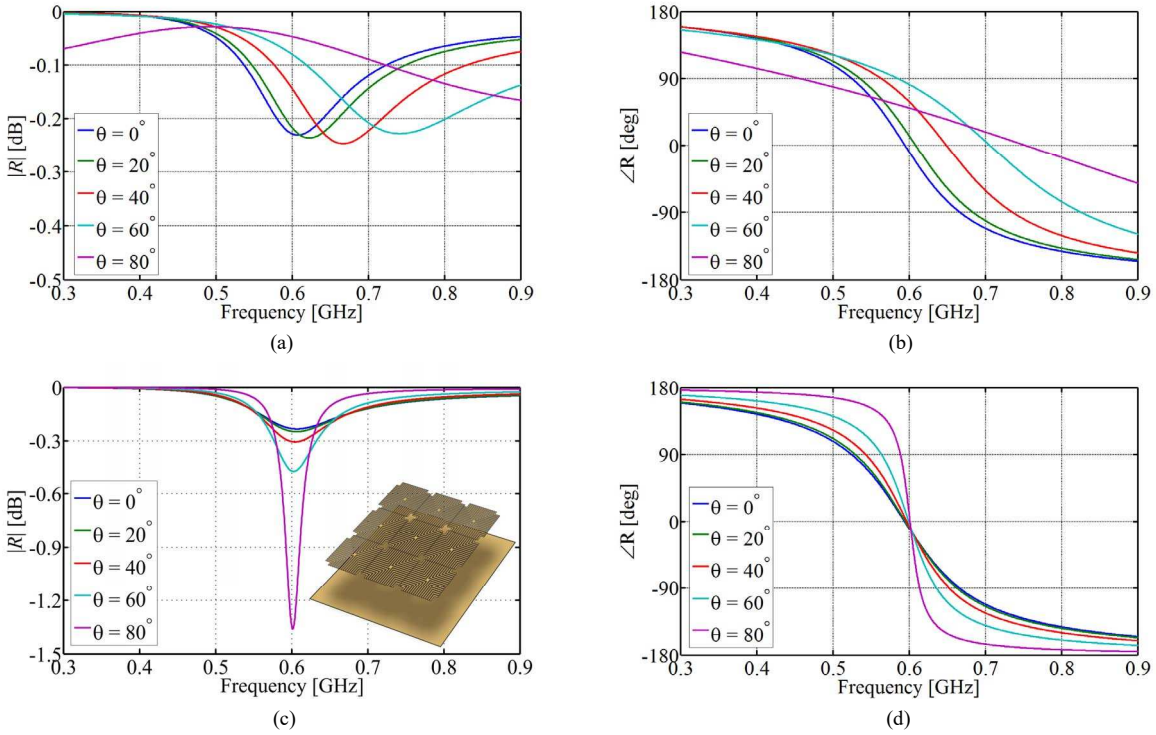

Fig. 12. Magnitude and phase of the reflection coefficient at normal and oblique incidence of (a)-(b) TM and (c)-(d) TE waves on the HIS with the fully interleaved Brigid's cross unit cell layout shown in Fig. 1.

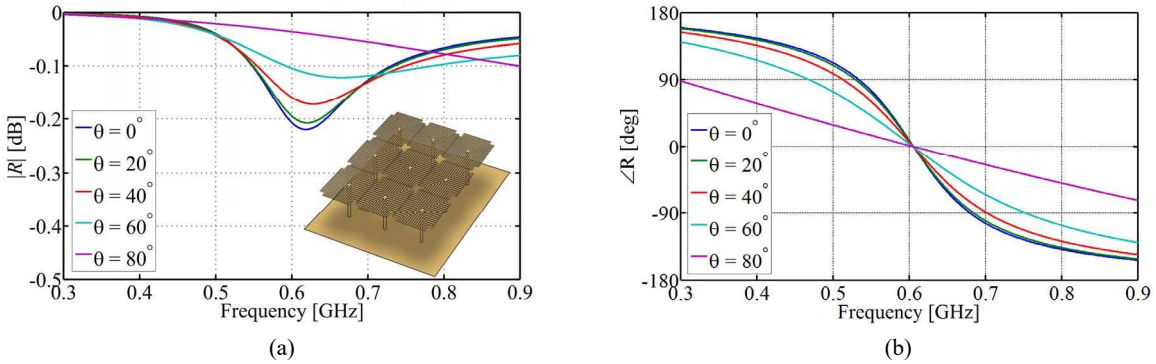

Fig. 13. Magnitude (a) and phase (b) of the reflection coefficient at normal and oblique incidence of TM waves on the modified HIS with the interleaved Brigid's crosses and additional conductor pins connected to the ground plane at the centre of each unit cell shown in inset.

bandwidth, which strongly depends on the unit cell layout. In this context interleaved Brigid's crosses, permitting somewhat independent control of f_r and FBW, allow broader FBW_{HIS} as demonstrated in Section IIIB.

Angular dependent HIS attenuation may be caused by cross-polarisation and dissipation in the array conductors. To assess effects of these two factors, $|R|$ of cross-polarised waves has been evaluated at θ varying from 0° to 80°. The simulation results have shown that cross-polarisation remained below -40 dB at any θ, thus implying the dominant contribution of conductor losses in the array pattern.

IV. Conclusion

A class of metasurfaces with substantially sub-wavelength unit cells comprised of the arrays of interleaved Brigid's crosses with the arms interspersed and spirally wound in adjacent unit cells has been proposed and discussed. It has been shown that Brigid's crosses enable a broader FBW than the other layouts of interwoven arrays with a unit cell of the same size while maintaining the high angular and polarisation stability of the fundamental resonance. An important distinctive feature of the interleaved Brigid's cross array is that its resonance frequency f_r can vary over a broad frequency range with minor changes of the FBW. The simulated and measured transmittance and reflectance of the array are in very good agreement.

The main properties of the interleaved Brigid's cross arrays and the effect of the geometrical parameters and dielectric substrate on the fundamental resonance have been elucidated using the full-wave simulations combined with the TL model of the unit cell. It has been established that the tight coupling between arms of the interleaved Brigid's crosses causes near-field localisation in the close proximity of the array surface and enables broad FBW at the substantially sub-wavelength resonance response. The analysis of the array with a variable number of interleaved folds of Brigid's cross arms on different substrate permittivities has revealed that the capacitive and inductive reactances of the unit cell can be adjusted somewhat independently to tailor the metasurface performance.

The salient features of the interleaved Brigid's cross arrays are particularly attractive for the design of compact HIS. It has been demonstrated that such HISs with substantially sub-wavelength unit cells can achieve practically the same FBW as the respective patch HIS, whilst exhibiting superior angular and polarisation stability of the HIS response and close near-field confinement. The distinctive properties of the HIS formed by the arrays of interleaved conductors have been elucidated using the corrected equivalent circuit model. The mechanisms of angular and polarisation stability in the HIS with thin substrates studded by thin conductor pins have been explained and illustrated by the example of interleaved Brigid's cross HIS.

Finally, it is noteworthy that the broad FBW and high angular and polarisation stability of the interleaved Brigid's cross arrays are attainable with scalable unit cell dimensions tailored to the specified operational frequencies. This enables compact FSSs and HISs to be manufactured by low-cost ink-jet printing and wet etching techniques.

Appendix

The effect of vias/pins on angular stability of both TE and TM polarised waves has been considered for the conventional HISs in earlier publications [3, 23, 24]. The Jerusalem cross and convoluted spiral HISs with pins have also been analysed and compared with the mushroom HIS in [25].

For discussion to be self-contained, it is expedient to briefly outline the physical mechanisms underlying the angular and polarisation stability of HISs comprised of interleaved conductor arrays backed by *thin* grounded dielectric layer studded by vias/pins. The input impedances of TE and TM waves obliquely incident at angle θ on a grounded dielectric slab of thickness t_s and permittivity ε_d have the form

$$Z_{in}^{\left\{\begin{smallmatrix}TE\\TM\end{smallmatrix}\right\}} = j\eta_0 \begin{cases} \dfrac{k_0}{k_y}\tan\left(k_y t_s\right), \text{ TE-wave} \\ \dfrac{k_y}{k_0}\tan\left(k_y t_s\right), \text{ TM-wave} \end{cases} \tag{7}$$

where $k_y = k_0\sqrt{\varepsilon_d - \sin^2\theta}$, k_0 and η_0 are the free space wavenumber and impedance, respectively. When a dielectric layer is sufficiently thin, i.e. $k_y t_s \ll 1$, the impedances can be approximated as follows

$$\begin{aligned} Z_{in}^{TE} &= j\eta_0 k_0 t_s\left[1 + O\left(\left(k_0 t_s\right)^2\left(\varepsilon_d - \sin^2\theta\right)\right)\right] \\ Z_{in}^{TM} &= j\eta_0 k_0 t_s\left(\varepsilon_d - \sin^2\theta\right)\left[1 + O\left(\left(k_0 t_s\right)^2\left(\varepsilon_d - \sin^2\theta\right)\right)\right] \end{aligned} \tag{8}$$

It is evident in (8) that Z_{in}^{TE} weakly depends on θ at $k_0 t_s \ll 1$, whilst Z_{in}^{TM} noticeably varies with θ even when the dielectric layer is very thin. To mitigate the latter issue in conventional HIS, it was suggested to connect the array conductors to ground by thin pins, like in mushroom HIS. Such periodic pins form a wire medium [23]. Since the electric field of TE wave is normal to the pins, it is weakly perturbed by short pins. Conversely, TM wave cannot propagate in the wire medium but it excites a TEM wave guided by the pins. The equivalent impedance of the TEM wave referenced to the surface of the grounded wire-medium slab is

$$Z_{in}^{TEM} = j\eta_0 k_0 \frac{\tan\left(k_0\sqrt{\varepsilon_d}\,t_s\right)}{k_0\sqrt{\varepsilon_d}} = j\eta_0 k_0 t_s\left[1 + O\left(\left(k_0 t_s\right)^2 \varepsilon_d\right)\right] \tag{9}$$

It is important to note in (9) that Z_{in}^{TEM} is angular independent and equal to Z_{in}^{TE} in the first approximation.

While the pins improve the angular stability of conventional HISs, the operational frequency of TM wave still considerably varies with θ as seen in [25]. The latter deviations are caused by the evanescent field of TM wave existing along with the TEM wave at the interface of the pin studded electrically thin dielectric layer. For the evanescent field to extinct at the scale much smaller than the layer thickness, it is necessary that

(i) near-field be closely confined to the layer surface and
(ii) wire-medium be dense, i.e. spacing between pins be much smaller than a wavelength in dielectric slab [23].

Fulfilling both the conditions simultaneously is impossible in the conventional square patch HIS where the unit cell size is not small enough to meet condition (ii). Alternatively, the arrays of interleaved conductors with substantially sub-wavelength unit

cells satisfy both the conditions. This is illustrated by Fig. 7 for the interleaved Brigid's crosses with the near-field closely confined to the gaps between strip conductors. The small periodicity of the array ($p < \lambda_s/23$, where λ_s is the wavelength in a dielectric substrate) makes the pin spacing substantially sub-wavelength that meets the wire-medium requirements.

This qualitative analysis is valid for any periodic arrays based upon interleaved conductor patterns which satisfy conditions (i)-(ii) above. As mentioned earlier, the interleaved Brigid's crosses are discussed here only as an illustrative example of such a HIS, and the presented qualitative theory is corroborated by the simulation results in Figs. 12, 13.

ACKNOWLEDGEMENT

The authors acknowledge partial support for this work by the EU FP7 Marie Curie IAPP project "WiFEEB–Wireless Friendly Energy Efficient Buildings", grant no. 286333.

REFERENCES

[1] B. A. Munk, *Frequency Selective Surfaces: Theory and Design*, New York: Wiley, 2000.
[2] D. Sievenpiper, L. Zhang, R. F. Jimene Broas, N. G. Alexopolous, and E. Yablonovitch, "High-impedance electromagnetic surfaces with a forbidden frequency band," *IEEE Trans. Microwave Theory Tech.*, vol. 47, no. 11, pp. 2059–2074, Nov. 1999.
[3] C. R. Simovski, P. de Maagt, S. A. Tretyakov, M. Paquay, and A. A. Sochava, "Angular stabilisation of resonant frequency of artificial magnetic conductors for TE-incidence," *Electron. Lett*., vol. 40, no. 2, Jan. 2004.
[4] Bilotti, F.; Toscano, A.; Vegni, L., "Design of spiral and multiple split-ring resonators for the realization of miniaturized metamaterial samples," *IEEE Trans. Antennas Propagt*., vol.55, no.8, pp.2258-2267, Aug. 2007.
[5] Bilotti, F.; Toscano, A.; Vegni, L.; Aydin, K.; Alici, Kamil Boratay; Ozbay, E., "Equivalent-Circuit Models for the Design of Metamaterials Based on Artificial Magnetic Inclusions," *IEEE Trans. Microwave Theory Tech.*, vol.55, no.12, pp.2865-2873, Dec. 2007.
[6] S. Barbagallo, A. Monorchio, and G. Manara, "Small periodicity FSS screens with enhanced bandwidth performance," *Electron. Lett*., vol. 42, pp. 382–384, March 2006.
[7] F. Huang, J. C. Batchelor and E. A. Parker, "Interwoven convoluted element frequency selective surfaces with wide bandwidths," *Electron. Lett*., vol. 42, pp. 788-790, July 2006.
[8] B. Sanz-Izquierdo, E. A. Parker, J.-B. Robertson, and J. C. Batchelor, "Singly and dual polarized convoluted frequency selective structures," *IEEE Trans. Antennas Propagat*., vol. 58, no.3, pp. 690-696, March 2010.
[9] A. Vallecchi and A. G. Schuchinsky, "Entwined spirals for ultra compact wideband frequency selective surfaces," *Proc. 4th European Conference on Antennas and Propagation*, *EuCAP 2010*, Barcelona, Spain, 12-16 Apr. 2010, A18P2-5.
[10] A. Vallecchi and A. G. Schuchinsky, "Entwined planar spirals for artificial surfaces," *IEEE Antennas Wireless Propagat. Lett*., vol. 9, pp. 994-997, 2010.
[11] A. Vallecchi and A. G. Schuchinsky, "Metasurfaces with intertwined conductor patterns," *Proceedings of Metamaterials' 2011*, Barcelona, Spain, 10-15 October 2011.
[12] A. Vallecchi and A. G. Schuchinsky, "Artificial surfaces formed by tessellations of intertwined spirals," *Proc. 5th European Conference on Antennas and Propagation*, *EuCAP 2011*, Rome, Italy, 11-15 April 2011, pp. 1846-1848.
[13] A. Vallecchi, R. J. Langley, A. G. Schuchinsky, "Voltage Controlled Intertwined Spiral Arrays for Reconfigurable Metasurfaces," *Int. Journal of Antennas and Propagation*, 171637, 2014.
[14] Bayraktar, Z.; Turpin, J.P.; Werner, D.H., "Nature-inspired optimization of high-impedance metasurfaces with ultrasmall interwoven unit cells," *IEEE Antennas Wireless Propagat. Lett*., vol.10, pp.1563-1566, 2011
[15] http://en.wikipedia.org/wiki/Brigid's_cross.
[16] P. Callaghan, E. A. Parker, R. J. Langley, "Influence of supporting dielectric layers on the transmission properties of frequency selective surfaces," *IEE Proc., H*, vol. 138, no. 5, pp. 448–454, 1991.
[17] F. C. Smith, B. Chambers, and J. C. Bennett, "Calibration techniques for free space reflection coefficients measurements," *Proc. Inst. Elect. Eng.*, vol. 139, no. 5, pp. 247–253, Sep. 1992.
[18] H. Mosallaei and K. Sarabandi, "Antenna miniaturization and bandwidth enhancement using a reactive impedance substrate," *IEEE Trans. Antennas Propagt*., vol. 52, no .9, pp. 2403-2414, Sep. 2004.
[19] A. Vallecchi, J. R. De Luis, F. Capolino, and F. De Flaviis, "Low profile fully planar folded dipole antenna on a high impedance surface," *IEEE Trans. Antennas Propagat*., vol. 60, no. 1, pp. 51-62, Jan. 2012.
[20] F. Costa, S. Genovesi, and A. Monorchio, "On the bandwidth of high-impedance frequency selective surfaces," *IEEE Antennas Wireless Propag. Lett.*, vol. 8, pp. 1341–1344, 2009.
[21] G.A. Korn and T.M. Korn, *Mathematical Handbook*. New York: McGraw-Hill, 1968.
[22] A. Vallecchi and A. G. Schuchinsky, "Analytical model of interwoven spiral arrays," *IET Microwave, Antennas & Propagat.*, vol. 8, no. 15, pp. 1268-1276, 2014.
[23] S. Tretyakov, *Analytical Modeling in Applied Electromagnetics*. Norwood, MA: Artech House, 2003.
[24] S.M. Hashemi, S.A. Tretyakov, M. Soleimani, C.R. Simovski, "Dual-Polarized Angularly Stable High-Impedance Surface," *IEEE Trans. Antennas Propagat*., vol. 61, no.8, pp.4101-4108, Aug. 2013.
[25] C.R. Simovski, P. de Maagt, I.V. Melchakova, "High-impedance surfaces having stable resonance with respect to polarization and incidence angle," *IEEE Trans. Antennas Propagat*., vol. 53, no.3, pp.908-914, March 2005.

Andrea Vallecchi received the Laurea (MSc) degree (summa cum laude) in electronic engineering from the University of Florence, Florence, Italy, and the Ph.D. degree in information engineering, applied electromagnetics, and telecommunications from the University of Salerno, Salerno, Italy. After a period as a research associate at the Laboratory of Antennas and Microwaves of the University of Florence, Italy, in 2008 he joined the University of Siena, Italy, as a postdoctoral research fellow. In 2013 he was awarded a Marie Curie research fellowship at the University of Sheffield, UK. He has been a Visiting Research Fellow at Queen's University of Belfast, Belfast, UK, on several occasions, and visiting researcher at the University of California, Irvine, US, in 2009. He was co-recipient of the "Best Antenna Theory Paper Award" at the *8th European Conference on Antennas and Propagation* in 2014. He is currently with the Department of Engineering Science, University of Oxford, UK. His research interests include the theoretical modelling and design of metamaterials, metasurfaces, and metamaterial-inspired antennas for applications at microwaves, THz, and optical frequencies.

Richard Langley (M'97–SM'12) has BSc and PhD degrees from the University of Kent. After spending some time working on communications satellites at Marconi Space Systems in the 1970s he became an academic at the University of Kent in 1979. Richard was Honorary Editor of IEE Proceedings – Microwaves, Antennas and Propagation from 1995-2003. In 1997 he founded the European Technology Centre for Harada Industries Japan, a global leader in automotive antennas. After successfully building up the technology and business he rejoined academic life in 2003. Professor Langley is now Head of the Communications Research Group and Director of Research in the EEE Department at the University of Sheffield. His main research is in the fields of automotive antennas, propagation in the built environment, frequency selective surfaces, electromagnetic band gap materials and applications, multi-function antenna systems and reconfigurable antennas. He initiated the setting up of the Wireless Friendly Building Forum in 2009 to address the problems of wireless signal propagation in buildings and the built environment. Richard has published over 350 papers in international journals and conferences and is a past Chair of the IET Antennas and Propagation Professional Network.

Alexander G. Schuchinsky (M'97–SM'05-F'14) received PhD degree in Radiophysics from Leningrad Electrotechnical Institute the academic title of Senior Research Scientist (USSR). He was Leading Scientist at the Microwave Electrodynamics Laboratory of Rostov State University, Russia and a Chief Engineer at Deltec-Telesystems, New Zealand. In 2002-2015 he was with the School of Electronics, Electrical Engineering and Computer Science, the Queen's University of Belfast, UK. He has published 3 international patents, 4 book chapters and over 200 refereed journal and conference papers. He was co-recipient of the IEEE 2010 Microwave Prize and received 2012 V.G. Sologub Award for contribution to Computational Electromagnetics. His main research interests include physics based modelling of linear and nonlinear phenomena in complex electromagnetic structures, metamaterials and nonreciprocal devices; passive intermodulation effects; and characterization of electromagnetic materials. He was a co-founder and General Co-Chair of the annual conference series "Metamaterials: International Congress on Advanced Electromagnetic Materials in Microwaves and Optics" and is a member of the Board of Directors of the Virtual Institute for Artificial Electromagnetic Materials and Metamaterials, "Metamorphose VI".